THE JOURNAL OF PHYSICAL CHEMISTRY A

ARTICLE

pubs.acs.org/JPCA

Coupled-Channels Quantum Theory of Electronic Flux Density in Electronically Adiabatic Processes: Application to the Hydrogen Molecule Ion

D. J. Diestler,[*,†,‡] A. Kenfack,[*,†] J. Manz,[†] and B. Paulus[†]

[†]Institut für Chemie und Biochemie, Freie Universität Berlin, 14195 Berlin, Germany

[‡]University of Nebraska—Lincoln, Lincoln, Nebraska 68583, United States

ABSTRACT: This article presents the results of the first quantum simulations of the electronic flux density ($\mathbf{j}_e$) by the "coupled-channels"(CC) theory, the fundamentals of which are presented in the previous article [Diestler, D. J. *J. Phys. Chem. A* **2012**, DOI: 10.1021/jp207843z]. The principal advantage of the CC scheme is that it employs exclusively standard methods of quantum chemistry and quantum dynamics within the framework of the Born−Oppenheimer approximation (BOA). The CC theory goes beyond the BOA in that it yields a nonzero $\mathbf{j}_e$ for electronically adiabatic processes, in contradistinction to the BOA itself, which always gives $\mathbf{j}_e = 0$. The CC is applied to oriented H_2^+ vibrating in the electronic ground state ($^2\Sigma_g^+$), for which the nuclear and electronic flux densities evolve on a common time scale of about 22 fs per vibrational period. The system is chosen as a touchstone for the CC theory, because it is the only one for which highly accurate flux densities have been calculated numerically without invoking the BOA [Barth et al, *Chem. Phys. Lett.* **2009**, *481*, 118]. Good agreement between CC and accurate results supports the CC approach, another advantage of which is that it allows a transparent interpretation of the temporal and spatial properties of $\mathbf{j}_e$.

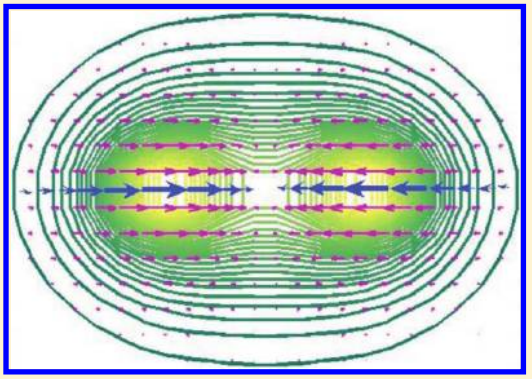

1. INTRODUCTION

Recent experimental observations of electronic motions in molecules on a time scale ranging from hundreds of attoseconds to a few femtoseconds[1] have inspired corresponding quantum-dynamical model simulations of coherent electronic and nuclear motions.[2−5] Especially germane to the present work is the proposal of a complex "time-shift flux", which provides an interesting picture of electronic flux densities during electronically *nonadiabatic* processes.[6] However, the computation of electronic flux densities ($\mathbf{j}_e$) that accompany electronically *adiabatic* processes, in particular, vibration and dissociation of molecules and molecular ions in the electronic ground state, remains a challenge. The description of such processes has traditionally been predicated on the Born−Oppenheimer approximation (BOA). On the one hand, the BOA, which is the basis of standard methods of quantum chemistry and quantum dynamics, successfully provides electronic and nuclear densities, as well as *nuclear* flux densities. On the other hand, it always yields $\mathbf{j}_e = \mathbf{0}$. Until recently, the only way to obtain nonzero $\mathbf{j}_e$s has been through extremely demanding brute-force computational methods that do not invoke the BOA. Only for the simplest system, namely, oriented H_2^+ vibrating in the electronic ground state ($^2\Sigma_g^+$), has a nonzero $\mathbf{j}_e$ been published.[7] We note by the way that it is much easier to compute the electronic flux (i.e., the "integrated" $\mathbf{j}_e$).[7−10]

One approach to the computation of nonzero $\mathbf{j}_e$ within the framework of the standard BOA-based methods is via an extension of the BOA that leads to a "coupled-channels" (CC) theory, the basics of which are presented in the previous article[11] (hereafter referred to as I). The relevant background is reviewed there[11] and elsewhere.[6−10] The present article (II) reports the results of the first CC quantum simulations of $\mathbf{j}_e$ for H_2^+. The reason for our choice of this system is that it is the *only* one for which highly accurate numerical $\mathbf{j}_e$s are available.[7] These accurate results provide a yardstick by which the accuracy of the approximate $\mathbf{j}_e$ predicted by the CC theory can be measured.

2. DESCRIPTION OF SYSTEM AND EQUATIONS OF MOTION

The quantum Hamiltonian of H_2^+ can be written

$$H = -\frac{\hbar^2}{2m_e}\nabla_{\mathbf{r}_e}^2 - \frac{\hbar^2}{2M_p}\nabla_{\mathbf{R}_a}^2 - \frac{\hbar^2}{2M_p}\nabla_{\mathbf{R}_b}^2 + V_c(\mathbf{r}_e, \mathbf{R}_a, \mathbf{R}_b) \tag{1}$$

where the Coulombic potential energy is given by

$$V_c = \frac{e^2}{4\pi\varepsilon_0}\left[\frac{1}{|\mathbf{R}_b - \mathbf{R}_a|} - \frac{1}{|\mathbf{r}_e - \mathbf{R}_a|} - \frac{1}{|\mathbf{r}_e - \mathbf{R}_b|}\right] \tag{2}$$

Special Issue: Femto10: The Madrid Conference on Femtochemistry

Received: August 15, 2011
Revised: October 19, 2011
Published: November 21, 2011

In eqs 1 and 2, $\mathbf{r}_e$, $\mathbf{R}_a$, and $\mathbf{R}_b$ are the positions of the electron (e) and protons (a,b) relative to the fixed laboratory reference frame; m_e and M_p are the respective masses of the electron and proton; e is the magnitude of the charge on the electron (proton); ε_0 is the permittivity of vacuum. Introducing the Jacobi coordinates

$$\begin{aligned} \mathscr{R} &= [m_e\mathbf{r}_e + M_p(\mathbf{R}_a + \mathbf{R}_b)]/M \\ \mathbf{r} &= \mathbf{r}_e - (\mathbf{R}_a + \mathbf{R}_b)/2 \\ \mathbf{R} &= \mathbf{R}_b - \mathbf{R}_a \end{aligned} \tag{3}$$

we can recast H as

$$H = -\frac{\hbar^2}{2M}\nabla^2_{\mathscr{R}} - \frac{\hbar^2}{2\mu_n}\nabla^2_{\mathbf{R}} - \frac{\hbar^2}{2\mu_e}\nabla^2_{\mathbf{r}} + V_c(\mathbf{r},\mathbf{R}) \tag{4}$$

where

$$V_c = \frac{e^2}{4\pi\varepsilon_0}\left[\frac{1}{R} - \frac{1}{|\mathbf{r} + \mathbf{R}/2|} - \frac{1}{|\mathbf{r} - \mathbf{R}/2|}\right] \tag{5}$$

The masses in eq 4 are $M = m_e + 2M_p$, $\mu_n = M_p/2$, and $\mu_e = 2m_eM_p/M$.

Note that the contribution of the total center of mass (c.o.m., $\mathscr{R}$) separates from that of the internal coordinates ($\mathbf{r}$,$\mathbf{R}$) in eq 4. Therefore, we can express the total wave function

$$\Psi(\mathscr{R},\mathbf{r},\mathbf{R},t) = \xi(\mathscr{R},t)\psi(\mathbf{r},\mathbf{R},t) \tag{6}$$

as a product of c.o.m. (ξ) and internal (ψ) factors, which satisfy the separate (time-dependent) Schrödinger equations

$$-\frac{\hbar^2}{2M}\nabla^2_{\mathscr{R}}\xi(\mathscr{R},t) = i\hbar\frac{\partial\xi(\mathscr{R},t)}{\partial t} \tag{7a}$$

$$\left[-\frac{\hbar^2}{2\mu_n}\nabla^2_{\mathbf{R}} - \frac{\hbar^2}{2\mu_e}\nabla^2_{\mathbf{r}} + V_c(\mathbf{r},\mathbf{R})\right]\psi(\mathbf{r},\mathbf{R},t) = i\hbar\frac{\partial\psi(\mathbf{r},\mathbf{R},t)}{\partial t} \tag{7b}$$

Equations 7a and 7b, respectively, govern the evolution of the wavepackets describing the c.o.m. and internal motion.

We desire to compute the "internal" flux densities (i.e., the flux density of the electron with respect to the nuclear c.o.m. (NCM) and the flux density of one nucleus with respect to the other) rather than "external" flux densities of electron and nuclei with respect to the origin of the laboratory frame. The classical expressions for the sought quantities are

$$\mathbf{j}_{e,\mathrm{NCM}}(\mathbf{x}',\mathbf{t}) = \boldsymbol{\delta}[\mathbf{x}' - \mathbf{r}(t)]\dot{\mathbf{r}}(t) \tag{8a}$$

$$\mathbf{j}_{b,a}(\mathbf{x},t) = \delta[\mathbf{x} - \mathbf{R}(t)]\dot{\mathbf{R}}(t) \tag{8b}$$

In eq 8a, $\mathbf{x}'$ is the point of observation relative to the NCM (i.e., the observer is stationed on the NCM); in eq 8b, $\mathbf{x}$ is the point of observation relative to the nucleus a (that is, the observer stands on nucleus a); $\dot{\mathbf{r}}$ and $\dot{\mathbf{R}}$ are the respective velocities of the electron relative to the NCM and of nucleus b relative to nucleus a. Note that we could as well compute the nuclear flux density of a relative to b. The two are identical and correspond to the flux density of one nucleus with respect to the other. The quantum expectation values corresponding to the classical expressions in eq 8 are

$$\langle\mathbf{j}_{e,\mathrm{NCM}}(\mathbf{x}',t)\rangle = \mathrm{Re}\{\langle\Psi(t)|\delta[\mathbf{x}' - \mathbf{r}]\dot{\mathbf{r}}|\Psi(t)\rangle\}$$

$$= \frac{\hbar}{2i\mu_e}\int d\mathbf{R}[\psi^*(\mathbf{r},\mathbf{R},t)\nabla_{\mathbf{r}}\psi(\mathbf{r},\mathbf{R},t) - \mathrm{c.c.}]_{\mathbf{r}=\mathbf{x}'} \tag{9a}$$

$$\langle\mathbf{j}_{b,a}(\mathbf{x},t)\rangle = \mathrm{Re}\{\langle\Psi(t)|\delta[\mathbf{x} - \mathbf{R}]\dot{\mathbf{R}}|\Psi(t)\rangle\}$$

$$= \frac{\hbar}{2i\mu_n}\int d\mathbf{r}[\psi^*(\mathbf{r},\mathbf{R},t)\nabla_{\mathbf{R}}\psi(\mathbf{r},\mathbf{R},t) - \mathrm{c.c.}]_{\mathbf{R}=\mathbf{x}} \tag{9b}$$

where "c.c." denotes the complex conjugate of the preceding term.

3. COUPLED-CHANNELS THEORY

Under the BOA, which assumes that the very light, fast electron responds instantly to the motion of the massive, sluggish nuclei, the wave function for the internal motion is expressed approximately as the single product

$$\psi(\mathbf{r},\mathbf{R},t) \simeq \Phi(\mathbf{r};\mathbf{R})\chi(\mathbf{R},t) \tag{10}$$

where Φ and χ satisfy the equations

$$\left[-\frac{\hbar^2}{2m_e}\nabla^2_{\mathbf{r}} + V_c(\mathbf{r},\mathbf{R})\right]\Phi(\mathbf{r};\mathbf{R}) = E(R)\Phi(\mathbf{r};\mathbf{R}) \tag{11a}$$

$$\left[-\frac{\hbar^2}{2\mu_n}\nabla^2_{\mathbf{R}} + E(R)\right]\chi(\mathbf{R},t) = i\hbar\frac{\partial\chi(\mathbf{R},t)}{\partial t} \tag{11b}$$

Here Φ is the (real) energy eigenfunction of the electron moving in the field of the nuclei at fixed separation $\mathbf{R}$. The energy eigenvalue $E(R)$ is parametric in $\mathbf{R}$ and by symmetry depends only on its magnitude. It is the effective potential energy surface for the relative motion of the nuclei, which is determined by the nuclear wavepacket χ.

Substitution of the approximate BOA wave function (eq 10) into eqs 9a and 9b yields

$$\langle\mathbf{j}_{e,\mathrm{NCM}}(\mathbf{x}',t)\rangle_{\mathrm{BOA}} = 0 \tag{12a}$$

$$\langle\mathbf{j}_{b,a}(\mathbf{x},t)\rangle_{\mathrm{BOA}} = \frac{\hbar}{2i\mu_n}[\chi^*(\mathbf{R},t)\nabla_{\mathbf{R}}\chi(\mathbf{R},t) - \mathrm{c.c.}]_{\mathbf{R}=\mathbf{x}} \tag{12b}$$

To circumvent the nonplussing result in eq 12a, we propose the CC theory in I.[11] Desiring to avail ourselves of the existing infrastructure of quantum chemistry, we suppose that the BOA electronic eigenfunction can be written

$$\Phi(\mathbf{r};\mathbf{R}) = \sum_{\alpha=a,b}\Phi_\alpha(\mathbf{r};\mathbf{R}) \tag{13}$$

where

$$\Phi_\alpha(\mathbf{r};\mathbf{R}) \equiv \sum_{l_\alpha} c_{l_\alpha}(R)\psi_{l_\alpha}(\mathbf{r},\mathbf{R}), \quad \alpha = a,b \tag{14}$$

and the ψ_{l_α} stand for atomic orbitals centered on nucleus α. For example, the (normalized) hydrogenic 1s orbital centered on nucleus b is, in atomic units, $\psi_{1s_b}(\mathbf{r},\mathbf{R}) = \pi^{-1/2}\exp(-|\mathbf{r} - \mathbf{R}/2|)$. The c_{l_α} are constants to be determined by requiring that Φ be a solution of eq 11a. Equations 13 and 14 constitute the standard LCAO-MO Ansatz.[12] The procedure detailed in I yields the CC

dx.doi.org/10.1021/jp207844w |J. Phys. Chem. A 2012, 116, 2736–2742

analogue of eq 9a:

$$\langle \mathbf{j}_{e,NCM}(\mathbf{x},t)\rangle_{CC} = \frac{1}{2}\int d\mathbf{R}[\Delta_b(\mathbf{x};\mathbf{R}) - \Delta_a(\mathbf{x};\mathbf{R})]\langle \mathbf{j}_{b,a}(\mathbf{R},t)\rangle_{BOA} \tag{15}$$

where $\langle \mathbf{j}_{b,a}(\mathbf{R},t)\rangle_{BOA}$ is given by eq 12b. In eq 15

$$\Delta_\alpha(\mathbf{r};\mathbf{R}) \equiv \Phi(\mathbf{r};\mathbf{R})\Phi_\alpha(\mathbf{r};\mathbf{R}), \quad \alpha = a,b \tag{16}$$

is the effective electronic probability (population) density associated with nucleus α.

From eqs 13 and 16, we have

$$\rho_e(\mathbf{r};\mathbf{R}) \equiv [\Phi(\mathbf{r};\mathbf{R})]^2 = \sum_{\alpha=a,b}\Delta_\alpha(\mathbf{r};\mathbf{R}) \tag{17}$$

which can be interpreted as the probability (population) density of the electron in the field of the nuclei at fixed separation **R**.

Note that the integrand in eq 15 is a simple product of two factors. The first "static" factor, $[\Delta_b(\mathbf{x};\mathbf{R}) - \Delta_a(\mathbf{x};\mathbf{R})]/2$, can be computed by means of routine methods of quantum chemistry. The second "dynamic" factor, $\langle \mathbf{j}_{b,a}(\mathbf{R},t)\rangle_{BOA}$, can be determined by solving the (time-dependent) nuclear Schrödinger equation (eq 11b) numerically by standard techniques of quantum dynamics.

4. COMPUTATIONAL METHODS

To simplify the numerical treatment, we introduce two assumptions. First, we suppose that the H_2^+ molecule can be oriented so that the internuclear separation **R** is parallel with the z-axis of the laboratory reference frame. Therefore, if the nuclei are constrained to the z-axis in the internal reference frame, whose axes are parallel with those of the laboratory frame, then ψ is a function only of R, $\mathbf{r}$, and t. Second, we take the initial ($t = 0$) wave function to be of the form

$$\psi(\mathbf{r},R,t=0) = \Phi_0(\mathbf{r};R)\chi_0(R,t=0) \tag{18}$$

where Φ_0 stands for the $^2\Sigma_g^+$ ground state of H_2^+. Because Φ_0 is invariant under rotations of the molecule about the z-axis (i.e., Φ_0 is cylindrically symmetric), so is $\psi(\mathbf{r},R,t)$. Hence, under these assumptions, we can cast eqs 7b, 9a, 11b, 12b, and 15 in terms of cylindrical coordinates as

$$\left\{-\frac{\hbar^2}{2\mu_n}\frac{\partial^2}{\partial R^2} - \frac{\hbar^2}{2\mu_e}\left[\frac{\partial^2}{\partial r^2} + \frac{1}{r}\frac{\partial}{\partial r} + \frac{\partial^2}{\partial z^2} + V_e(r,z,R)\right]\right\}\psi(r,z,R,t) = i\hbar\frac{\partial\psi(r,z,R,t)}{\partial t} \tag{19a}$$

$$\langle \mathbf{j}_{e,NCM}(r,z,t)\rangle = \frac{\hbar}{2i\mu_e}\int_0^\infty dR\left[\psi^*(r,z,R,t)\frac{\partial\psi(r,z,R,t)}{\partial r} - c.c.\right]\mathbf{e}_r + \frac{\hbar}{2i\mu_e}\int_0^\infty dR\left[\psi^*(r,z,R,t)\frac{\partial\psi(r,z,R,t)}{\partial z} - c.c.\right]\mathbf{e}_z \equiv j_{er}(r,z,t)\mathbf{e}_r + j_{ez}(r,z,t)\mathbf{e}_z \tag{19b}$$

$$\left[-\frac{\hbar^2}{2\mu_n}\frac{\partial^2}{\partial R^2} + E_0(R)\right]\chi_0(R,t) = i\hbar\frac{\partial\chi_0(R,t)}{\partial t} \tag{19c}$$

$$\langle \mathbf{j}_{b,a}(R,t)\rangle_{BOA} = \frac{\hbar}{2i\mu_n}\left[\chi_0^*(R,t)\frac{\partial\chi_0(R,t)}{\partial R} - c.c.\right]\mathbf{e}_z \equiv j_n(R,t)\mathbf{e}_z \tag{19d}$$

$$\langle \mathbf{j}_{e,NCM}(r,z,t)\rangle_{CC} = \frac{1}{2}\int_0^\infty dR[\Delta_b(r,z;R) - \Delta_a(r,z;R)]j_n(R,t)\mathbf{e}_z \equiv j_{ez,CC}(r,z,t)\mathbf{e}_z \tag{19e}$$

where **e** signifies a unit vector and r now stands for the distance of the electron from the internuclear axis.

We note that by the very nature of the approximations invoked to reach eq 15 the CC electronic flux density ($\mathbf{j}_e$) is everywhere parallel with the nuclear flux density, which is parallel with the internuclear axis. Hence, because the nuclei are constrained to the z-axis, the CC $\mathbf{j}_e$ (eq 19e) has only a z-component, in contradistinction to the accurate $\mathbf{j}_e$ (eq 19b), which generally has both z- and r-components.[7] It turns out, however, that the z-component is by far the dominant one. Hence, the CC $\mathbf{j}_e$ accounts for the more significant component of the total flux density.[7] Most of the time (i.e., whenever the nuclear flux density j_n is unidirectional, corresponding to bond compression or bond stretching) the magnitude of the z-component of $\mathbf{j}_e$ exceeds that of the r-component by an order of magnitude.[7] The z-component is also about an order of magnitude larger in the "unidirectional" regime than it is in the exceptional event where the nuclear wavepacket $\chi_0(R,t)$ changes direction (analogous to the change of the direction of a classical trajectory close to a turning point). In these rare instances, both the z- and r-components may have similar values on a relative scale. On the absolute scale, however, the r-component always remains negligible compared to the maximum value of the z-component.

Using the Gaussian 03 package,[13] we perform Hartree−Fock calculations in the basis set aug-cc-pVDZ[14] to compute the ground-state wave function Φ_0 and energy $E_0(R)$ as a function of R. We find a minimum of $-0.60253E_h$ at $R_e = 2.00a_0$ in $E_0(R)$. Atomic units are used throughout the text, unless it is otherwise indicated.

We take the *initial* nuclear wavepacket to be $\chi_0(R,t=0) = \chi_{0,0}(R-\overline{R})$, where $\chi_{0,0}(R-\overline{R})$ is the ground-state vibrational energy eigenfunction translated in the positive R direction by $\overline{R}$. We set $\overline{R} = R_e = 2.00a_0$, because this is the only value for which accurate results are available.[7] The ground-state eigenfunction $\chi_{0,0}(R)$ is determined by solving the eigenvalue problem

$$\left[-\frac{\hbar^2}{2\mu_n}\frac{\partial^2}{\partial R^2} + E_0(R)\right]\chi_{0,0}(R) = W_{0,0}\chi_{0,0}(R) \tag{20}$$

which is done by propagating the wave function on a 256-point grid covering the range $0 \le R \le 16a_0$ in imaginary time for 10^3 steps of 0.0012 fs.[15]

The total initial wave function is then

$$\psi(r,z,R,t=0) = \Phi_0(r,z;R)\chi_{0,0}(R-\overline{R}) \tag{21}$$

It should be noted that the initial state, as described by the wave function in eq 21, is not a true eigenstate of the energy of the system. Indeed, the true state can be represented as a superposition of the BO electronic ground state (Φ_0) and BO electronic excited states ($\Phi_n, n > 0$). However, since the excited-state components decay within 2 or 3 fs, the initial wave function rapidly evolves into a wavepacket that reliably represents the electronic ground state over the relevant temporal and spatial domains.[7]

We propagate the nuclear wavepacket by the split-operator technique[16] on the same grid and with the same time step size employed in the determination of the vibrational ground state $\chi_{0,0}$. As a measure of the accuracy of the solution, we

monitor the norm

$$N(t) \equiv \int_0^\infty dR|\chi_0(R,t)|^2 \tag{22}$$

which remains equal to 1 within 0.002% throughout the vibrational period over which the packet is propagated. We also compute the mean value of the internuclear separation

$$\langle R(t)\rangle \equiv \int_0^\infty dR|\chi_0(R,t)|^2 R \tag{23}$$

Highly accurate numerical solutions of the Schrödinger equation (eq 19a) obtained by the method of Paramonov[17,18] for the initial wavefunction (eq 21) were previously computed on a grid with 50 points in the r-direction over the range $0.2208a_0 \le r \le 18.51a_0$ and 110 points in the z-direction over the range $-18.00a_0 \le z \le 18.00a_0$. The same grid is employed to represent the current CC quantities $\Delta_\alpha(r,z;R)$ and ρ_e.

Partial derivatives $\partial\psi(r,z,R,t)/\partial z$ and $\partial\chi_0(R,t)/\partial R$ required to calculate j_{ez} (eq 19b) and $j_n(R,t)$ (eq 19d), respectively, are computed on the above-described grids by central-difference formulas.[19] For example,

$$\partial\psi(r,z,R,t)/\partial z \simeq [\psi(r_i,z_{j+1},R_k,t_n) - \psi(r_i,z_{j-1},R_k,t_n)]/2\Delta z \tag{24}$$

where i, j, k, and n label points of the grid in the various dimensions and Δz is the spacing of the grid in the z-direction. The required integrations on R (see eqs 19b, 19e, 22, and 23) are done by the extended trapezoidal rule.[19]

5. RESULTS AND DISCUSSION

Equation 19e indicates that the CC $\mathbf{j}_e$ is essentially determined by the character of the integrand

$$I(r,z,R,t) \equiv p(r,z;R) \times j_n(R,t) \tag{25a}$$

where

$$p(r,z;R) \equiv \frac{1}{2}[\Delta_b(r,z;R) - \Delta_a(r,z;R)] \tag{25b}$$

can be viewed as the electronic "probability" distribution that is associated with the CC $\mathbf{j}_e$. Hence, the integrand is a simple product of factors p and j_n, which can be determined by standard procedures of quantum chemistry and quantum dynamics, respectively.

We first examine the quantum-chemistry factor p. Figure 1 illustrates the decomposition of the electronic probability density into the components Δ_α associated with the protons $\alpha = a,b$, according to eq 17. The anticipated symmetries

$$\rho_e(r,-z;R) = \rho_e(r,z;R) = \Delta_a(r,z;R) + \Delta_b(r,z;R) \tag{26a}$$

$$\Delta_a(r,-z;R) = \Delta_b(r,z;R) \tag{26b}$$

are apparent in Figure 1. At very large R (i.e., in the asymptotic region), $\Delta_\alpha \rightarrow (1/2)[\psi_{1s\alpha}([r^2 + (z \pm R/2)^2]^{1/2})]^2$, which corresponds to "one-half" of the electron being localized on each proton. As R decreases, $\Delta_\alpha$remains very nearly spherical and very nearly centered on proton α (a and b located at $z = -R/2$ and $z = R/2$, respectively), until the atomic orbitals on a and b begin to overlap and the distribution Δ_α begins to skew toward the other proton (i.e., the electron tends to be drawn between the protons).

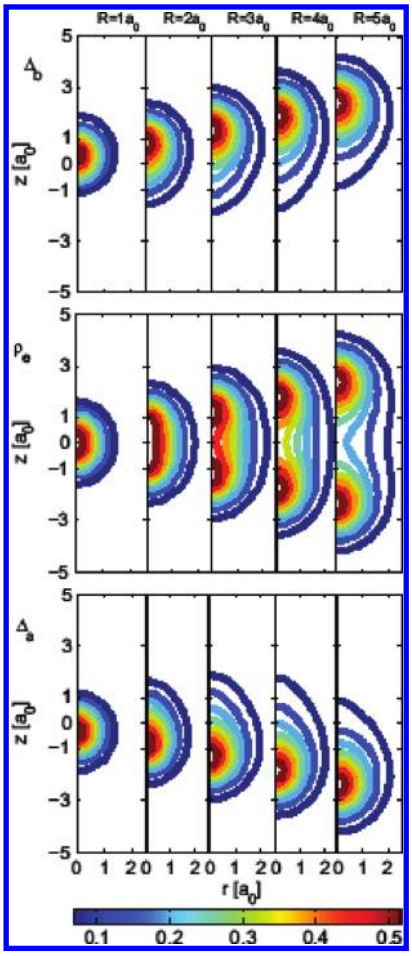

Figure 1. Contour plots of electron density and its components associated with protons a and b in the $z-r$ plane for several internuclear separations R for oriented H_2^+ in $^2\Sigma_g^+$ electronic ground state. Upper panel: Δ_b(eq 16); center panel: ρ_e (eq 17); bottom panel: Δ_a (eq 16).

From eqs 25b and 26b it follows that

$$p(r,-z;R) = -p(r,z;R) \tag{27}$$

That is, $z = 0$ is always a nodal plane of p. Also, as R increases from small R, the extent of orbital overlap declines and p bifurcates in the same way as ρ_e, except that the signs of the two components differ. In the asymptotic limit,

$$p(r,z;R) \rightarrow \frac{1}{2}\{[\psi_{1s_b}([r^2 + (z - R/2)^2]^{1/2})]^2 - [\psi_{1s_a}([r^2 + (z + R/2)^2]^{1/2})]^2\} \tag{28}$$

We turn next to the role of the quantum-dynamics factor $j_n(R,t)$. We consider results for three times corresponding to two different regimes of the nuclear motion: $t = t_1 = 6.45$ fs, when the peak of the nuclear probability density

$$\rho_n(R,t) = |\chi_0(R,t)|^2 \tag{29}$$

has moved about halfway from its initial location ($\langle R\rangle = 4a_0$) toward the point where the bond is shortest ($\langle R\rangle = 2a_0$) at $t = t_3 = 11.05$ fs; for an illuminating comparison, we include the situation at $t = t_2 = 11.00$ fs, just 50 as before t_3. The top panels of Figure 2

dx.doi.org/10.1021/jp207844w |J. Phys. Chem. A 2012, 116, 2736–2742

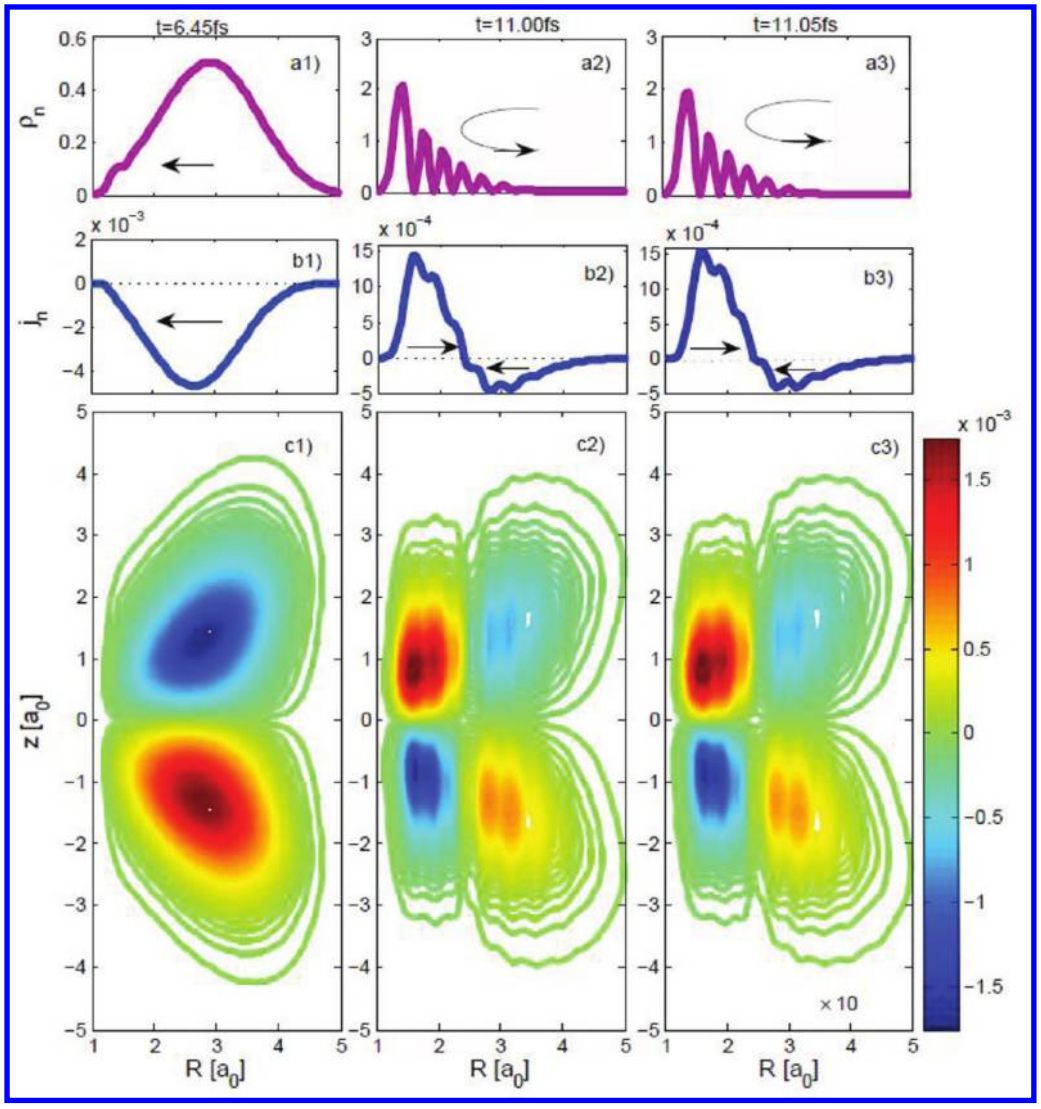

Figure 2. Results for oriented H_2^+ vibrating in $^2\Sigma_g^+$ electronic ground state. Panels a1−a3: Nuclear probability density ρ_n (eq 29) versus internuclear distance R at fixed $t = t_1 = 6.45$ fs (a1), $t = t_2 = 11.00$ fs (a2), and $t = t_3 = 11.05$ fs (a3). Arrows indicate directions of motion of nuclear wavepacket $\chi_0(R,t)$. (Note that scale for ordinate in (a1) differs from that in (a2) and (a3).) Panels b1−b3: Nuclear flux density j_n (eq 19d) vs R at t_1 (b1), t_2 (b2), and t_3 (b3). (Note that scale for ordinate in (b1) differs from that in (b2) and (b3).) Panels c1−c3: Contour diagrams of $I(r,z,R,t)$ (eq 25a) in $z-R$ plane at fixed $r = 0.22a_0$ and fixed $t = t_1$ (c1), $t = t_2$ (c2), and $t = t_3$ (c3).

display plots of ρ_n versus R at times t_1, t_2, and t_3; the center panels show plots of the corresponding (relative)j_n. For convenience in describing the evolving state of the system, we designate by "head", "center", and "tail" portions of $\chi_0(R,t)$ that refer to small, intermediate, and large values of R, respectively. At t_1, all three "parts" of $\chi_0(R,t)$ run in the same direction, corresponding to bond compression. Thus, $j_n(R,t_1)$ is negative for all R. In contrast, times t_2 and t_3 correspond to a change in the direction of motion of $\chi_0(R,t)$ from bond shortening to bond lengthening (analogous to a classical trajectory that changes direction at a classical turning point). This turning of $\chi_0(R,t)$ is accompanied by a systematic change in the shape of j_n. Because the behavior of j_n in the vicinity of the turning point is critical to the later analysis of discrepancies between the $j_{ez,CC}$ and j_{ez}, we presently describe the turning in depth.

The change of direction of motion of $\chi_0(R,t)$ starts with the turn of the "head," which is followed by turns of the "center" and finally of the "tail." As a consequence of the lags between turns of the three "parts", they overlap each other during the interval of turning of $\chi_0(R,t)$. This overlap causes interferences in $\rho_n(R,t)$, which are visible in panels a2 and a3 of Figure 2. The interferences are also reflected in oscillations superimposed on the otherwise relatively smooth $j_n(R,t)$ (see panels b2 and b3 of Figure 2). The beginning of the turn of the "head" occurs at rather small R, where the switch from negative to positive values of $j_n(R,t)$ can be seen. At the same time the "center" and the "tail" are still running from larger to smaller R, corresponding to negative values of $j_n(R,t)$ at larger R. Thus, the change from bond compression to bond stretching is associated with the appearance of a node at $R = R_{node}(t)$ in $j_n(R,t)$, which separates positive values of $j_n(R,t)$ for $R < R_{node}(t)$ from negative values for $R > R_{node}(t)$. As time proceeds, the "head" of $\chi_0(R,t)$ moves toward larger R and consequently the position of the node in $j_n(R,t)$ increases with time. During the same interval, the "center" and "tail" rebound, following the "head" toward increasing R. This means that the positive regime of $j_n(R,t)$, where $R < R_{node}(t)$,

dx.doi.org/10.1021/jp207844w |J. Phys. Chem. A 2012, 116, 2736–2742

grows (because the successive parts of $\chi_0(R,t)$ switch direction from bond compression to bond stretching) at the expense of the negative regime, where $R > R_{node}(t)$. This "leakage" from negative to positive regimes of $j_n(R,t)$ can be seen by comparing snapshots of $j_n(R,t_2)$ and $j_n(R,t_3)$ (panels b2 and b3 of Figure 2), which indicate that between t_2 and t_3 the node in $j_n(R,t)$ moves from $R_{node}(t_2) = 2.4a_0$ to $R_{node}(t_3) = 2.5a_0$. It is remarkable that these differences are visible, albeit on quite close inspection, in two snapshots separated by a mere 50 as. At the end of the interval of turning, the entire $\chi_0(R,t)$ is running toward larger R (i.e., the entire negative region of $j_n(R,t)$ has been converted into the positive one, and the node in $j_n(R,t)$ disappears).

From a classical perspective, the nuclear velocity at t_1 is negative and relatively large, whereas it becomes very small near the (inner) classical turning point, which corresponds to t_3. Therefore, $|j_n(R,t_1)|$ is about an order of magnitude larger than $|j_n(R,t_3)|$. (Note that the scale of the ordinate in panel b1 of Figure 2 differs from that in panels b2 and b3.)

The bottom panels of Figure 2 display projections of $I(r,z,R,t)$ (eq 25a) onto the $z-R$ plane at $r = 0.22a_0$. From the structure of the integrand I, which is a product of the antisymmetric (under reflection in the plane $z = 0$) p and j_n, it can be seen that $z = 0$ is a nodal plane of I in all cases. Accordingly, $I(r,z,R,t_1)$ (panel c1 of Figure 2) has two lobes, which extend along lines roughly parallel with the two diagonals $z = R$ and $z = -R$. These orientations of the lobes reflect the correlation between the locations of electrons and nuclei, as indicated by the probability distribution associated with the CC $\mathbf{j}_e$ (see eq 25b and Figure 1). Approximately the same correlations are also visible in the lobes of the integrands $I(r,z,R,t_2)$ and $I(r,z,R,t_3)$ (see panels c2 and c3 of Figure 2). We note, however, that $I(r,z,R,t_2)$ and $I(r,z,R,t_3)$, respectively, manifest nodes at $R_{node} = 2.4a_0$ and $R_{node} = 2.5a_0$, which are due to the nodes in $j_n(R,t_2)$ and $j_n(R,t_3)$ at the same R. Scrutiny of the integrands $I(r,z,R,t)$ at $t = t_2$ and $t = t_3$ also reveals an effect of the systematic increase of the positive region of $j_n(R,t)$ at the expense of the negative one: the corresponding lobes of $I(r,z,R,t_2)$ at small R ($R < R_{node}(t)$) enlarge from $t = t_2$ to $t = t_3$ at the expense of the lobes at larger R ($R > R_{node}(t)$).

Figures 3 and 4 display contour plots of $j_{ez,CC}(r,z,t)$ (eq 19e) and $j_{ez}(r,z,t)$ (eq 19b) at times t_1 and t_3, respectively. Figure 4 also displays a plot of $j_{ez,CC}(r,z,t)$ at time t_2. We note the substantial difference between the magnitudes of $j_{ez,CC}$ at times t_1 and t_3 (or t_2), which can be rationalized by inspection of the CC expression in eq 19e. It is clearly a direct consequence of the greater absolute value of $j_n(R,t)$ at t_1 than at t_3 (or t_2). Moreover, the nodal structure apparent in the plots of $j_{ez,CC}$ in Figures 3 and 4 can be explained in terms of the nodal structure visible in the plots of $I(r = 0.22a_0,z,R,t)$ in Figure 2. Imagine that vertical lines $r = 0.22a_0$ are drawn in the panels of Figures 3 and 4. Now observe that the value of $j_{ez,CC}$ ($r = 0.22a_0, z = c,t$) at the intersection of the line $z = c$ (where c is an arbitrary (real) constant) with the line $r = 0.22a_0$ is equal to

$$j_{ez,CC}(r = 0.22a_0, z = c, t) = \int_0^\infty dR I(r = 0.22a_0, z = c, R, t) \quad (30)$$

(i.e., the integral of I over R along the line $z = c$ in Figures 2c1 and c3). Thus, at t_1, this integral along any line for which $c \neq 0$ cannot vanish because I does not change sign. For $c < 0$, $j_{ez,CC}(r = 0.22a_0, z = c,t_1)$ is positive since $I(r = 0.22,z = c,R,t) \geq 0$. By analogous reasoning, $j_{ez,CC}(r = 0.22a_0,z = c,t_1)$ is negative for $c > 0$. When

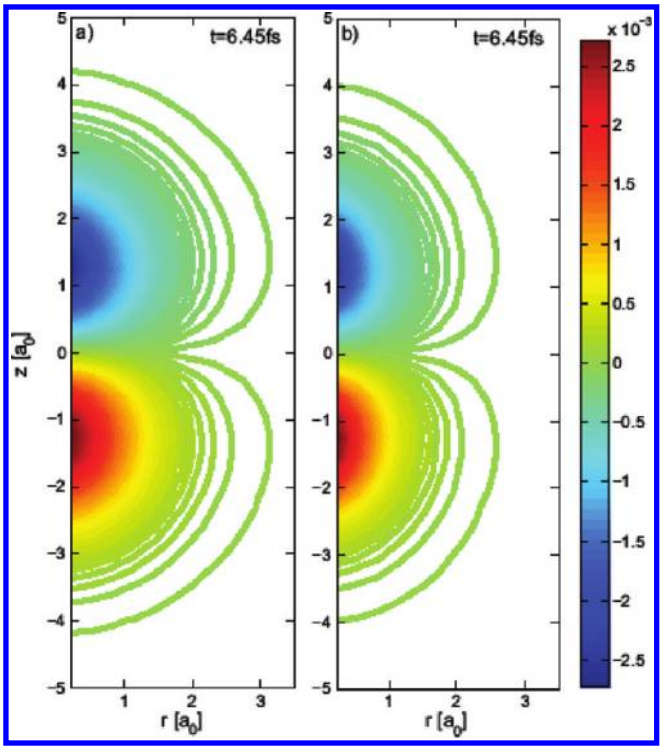

Figure 3. Results for oriented H_2^+ vibrating in $^2\Sigma_g^+$ electronic ground state. Contour plots of CC electronic flux density $j_{ez,CC}$ (eq 19e) (a) and accurate counterpart j_{ez} (eq 19b) (b) in $r-z$ plane at fixed $t = t_1 = 6.45$ fs.

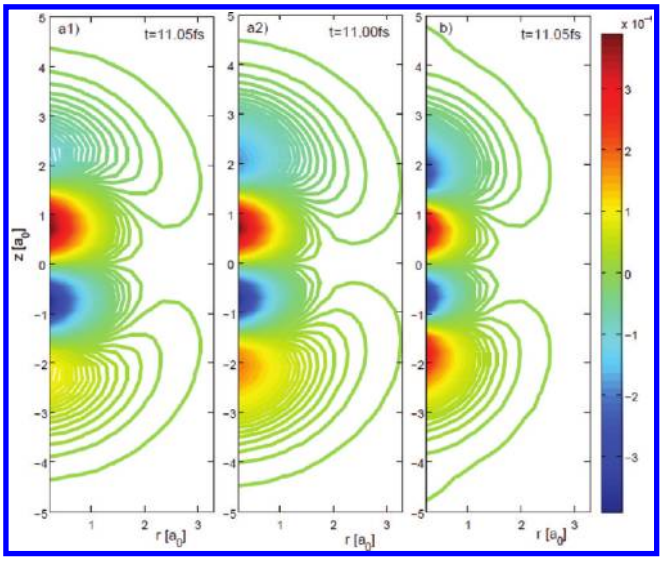

Figure 4. Same as Figure 3, except at fixed $t = t_3 = 11.05$ fs (panels a1 and b). Panel a2 shows CC electronic flux density at fixed $t = t_2 = 11.00$ fs.

$c = 0$, z is on the nodal plane and $I = 0$ for all R. At t_3, there is a nodal plane in I at $R \simeq 2.5\ a_0$ in addition to the one at $z = 0$. Thus, there exist values of the constant $c \neq 0$, where the integral in eq 30 vanishes. The plot $j_{ez,CC}(r = 0.22a_0,z = c,t_2)$ in Figure 4a1 shows nodes on the line $r = 0.22a_0$ around $c \simeq \pm 1.5a_0$. Visual inspection of the plot of $I(r = 0.22a_0,z,R,t_2)$ in Figure 2c3 suggests that the integral over the lines at $c \simeq \pm 1.5a_0$ should indeed vanish.

The apparent overall agreement between $j_{ez,CC}$ and j_{ez} is very good at t_1, when j_n is unidirectional, corresponding to pure bond

dx.doi.org/10.1021/jp207844w | J. Phys. Chem. A 2012, 116, 2736–2742

compression (Figure 3). Nevertheless, scrutiny of the contour diagrams in Figure 4 exposes slight disparities at t_3, when j_n is bidirectional, corresponding to the turning of $\chi_0(R,t)$. In particular, the maxima and minima of the four lobes of $j_{ez}(R,z,t_3)$ (Figure 4b) have approximately the same magnitude. In contrast, the absolute values of the four extrema of $j_{ez,CC}(R,z,t_3)$ (Figure 4a1) differ in that the two near $z = \pm 0.7a_0$ and $z = \pm 2a_0$ are slightly larger and smaller, respectively, than the corresponding extrema of $j_{ez}(R,z,t_3)$. To illuminate this discrepancy we compare $j_{ez,CC}(R,z,t_2)$ (Figure 4a2) and $j_{ez,CC}(R,z,t_3)$, which are separated by just 50 as. The agreement between $j_{ez,CC}(R,z,t_2)$ and $j_{ez}(R,z,t_3)$ is clearly better than that between $j_{ez,CC}(R,z,t_3)$ and $j_{ez}(R,z,t_3)$. This can be understood as a consequence of the time evolution of $j_n(R,t)$ and the resulting impact on the integrand $I(r,z,R,t)$ during the turn of the nuclear wavepacket $\chi_0(R,t)$. At the earlier time t_2, the regimes where $j_n(R,t_2)$ is positive ($R < R_{node}(t_2)$) or negative ($R > R_{node}(t_2)$) are, respectively, smaller and larger than they are at the later time t_3. Therefore, the lobes of $I(r,z,R,t_2)$ for $R < R_{node}(t_2)$ and $R > R_{node}(t_2)$ have, respectively, larger and smaller magnitudes than the lobes of $I(r,z,R,t_3)$ for $R < R_{node}(t_3)$ and $R > R_{node}(t_3)$ (see Figure 2). The overall directionality of the lobes of $I(r,z,R,t)$ then implies that the integration in eq 30 yields smaller and larger absolute values of the extrema for $j_{ez,CC}(r = 0.22a_0,z,t_2)$ close to $z = \pm 0.7a_0$ and $z = \pm 2a_0$, respectively, and hence better agreement between $j_{ez,CC}(r = 0.22a_0,z,t_2)$ and $j_{ez}(R,z,t_3)$ than between $j_{ez,CC}(r = 0.22a_0,z,t_3)$ and $j_{ez}(R,z,t_3)$.

The foregoing analysis highlights the extraordinary sensitivity of $j_{ez,CC}(R,z,t)$ to small shifts in the time, even in the attosecond domain. Moreover, it prompts a conjecture that the agreement between $j_{ez,CC}(R,z,t)$ and $j_{ez}(R,z,t)$ is almost quantitative, not only for times such as t_1, when the nuclear flux density is unidirectional, but even at times near the turning of the nuclear wavepacket, *if* one permits shifts of the order of a few attoseconds in the time between snapshots of accurate and CC results. We speculate that such tiny shifts may be correlated with the use different numerical methods for the propagation of the accurate wave function,[17,18] which inextricably entangles electronic and nuclear motions, and for the propagation of the nuclear wave function within the framework of the CC approach,[11] which is based on the BO separation of electronic and nuclear motions.

6. CONCLUSIONS

The results of our application of the coupled-channels (CC) theory to H_2^+, which demonstrate good overall agreement between CC and accurate results for j_{ez}, are gratifying. The CC formula for $j_{ez,CC}$ (see eq 19e) is especially useful for two reasons. First, it can be computed by exploiting the existing infrastructure of theoretical chemistry. The formula involves a simple product of two factors: p (eq 25b), a sort of electronic "probability" distribution, which can be determined from the BOA electronic eigenfunction obtained by standard techniques of quantum chemistry; and j_n (eq 19d), the (relative) nuclear flux density, which can be determined by solving the BOA nuclear Schrödinger equation by means of standard methods of quantum dynamics. The second reason is that the factorization permits valuable insight into the spatial and temporal structure of j_{ez}.

The current paper presents results only for the simplest system, because it is the only one for which highly accurate non-BOA electronic flux densities are currently available to serve as benchmarks for assessing the reliability of the CC results. The positive results instill hope that the CC approach can be extended to more complex systems. Additional applications are under consideration.

■ ACKNOWLEDGMENT

The authors are grateful to Dirk Andrae for helpful technical advice on the quantum chemistry computations. D.J.D. thanks the Freie Universität Berlin for support for several visits. J.M. thanks the Fonds der chemischen Industrie for continuous support.

■ REFERENCES

(1) Krausz, F.; Ivanov, M. *Rev. Mod. Phys.* **2009**, *81*, 163–234.
(2) Martin, F.; et al. *Science* **2007**, *315*, 629–633.
(3) Bandrauk, A. D.; Chelkowski, S.; Kawai, S.; Lu, H. *Phys. Rev. Lett.* **2008**, *101*, 153901−1–153901−4.
(4) Tseng, T.-C.; et al. *Nature Chem.* **2010**, *2*, 374–379.
(5) Bandrauk, A. D., Ivanov, M. Y., Eds. *Quantum Dynamic Imaging*; Springer: New York, 2011.
(6) Okuyama, M.; Takatsuka, K. *Chem. Phys. Lett.* **2009**, *476*, 109–115.
(7) Barth, I.; Hege, H.-C.; Ikeda, H.; Kenfack, A.; Koppitz, M; Manz, J.; Marquardt, F.; Paramonov, G. K. *Chem. Phys. Lett.* **2009**, *481*, 118–123.
(8) Kenfack, A.; Marquardt, F.; Paramonov, G, K.; Barth, I.; Lasser, C.; Paulus, B. *Phys. Rev. A* **2010**, *81*, 052502−1–052502−7.
(9) Kenfack, A.; Barth, I.; Marquardt, F.; Paulus, B. *Phys. Rev. A* **2010**, *82*, 062502−1–062502−7.
(10) Andrae, D.; Barth, I.; Bredtmann, T.; Hege, H.-C.; Manz, J.; Marquardt, F.; Paulus, B. *J. Phys. Chem. B* **2011**, *115*, 5476–5483.
(11) Diestler, D. J. *J. Phys. Chem. A* **2012**, DOI: 10.1021/jp207843z.
(12) Szabo, A; Ostlund, N. S. *Modern Quantum Chemistry: Introduction to Advanced Electronic Structure Theory*; Macmillan Publishing Co., Inc.: New York, 1982.
(13) Frisch, M. J. et al. *Gaussian 03*, Revision C.02; Gaussian, Inc.: Wallingford, CT, 2004.
(14) Dunning, T. H. *J. Chem. Phys.* **1989**, *90*, 1007–1023.
(15) Kosloff, R.; Tel-Ezer, H. *Chem. Phys. Lett.* **1986**, *127*, 223–230.
(16) Feit, M. D.; Fleck, J. A., Jr.; Steiger, A. *J. Comput. Phys.* **1982**, *47*, 412–433.
(17) Paramonov, G. K. *Chem. Phys. Lett.* **2005**, *411*, 350–356.
(18) Paramonov, G. K. *Chem. Phys.* **2007**, *338*, 329–341.
(19) Abramowitz, M; Stegun, I. A. *Handbook of Mathematical Functions*; U.S. Government Printing Office: Washington, D.C., 1965.